A Global Dataset of Palmer Drought Severity Index for 1870–2002: Relationship with Soil Moisture and Effects of Surface Warming

AIGUO DAI, KEVIN E. TRENBERTH, AND TAOTAO QIAN

National Center for Atmospheric Research, Boulder, Colorado*

(Manuscript received 24 February 2004, in final form 26 May 2004)

ABSTRACT

A monthly dataset of Palmer Drought Severity Index (PDSI) from 1870 to 2002 is derived using historical precipitation and temperature data for global land areas on a 2.5° grid. Over Illinois, Mongolia, and parts of China and the former Soviet Union, where soil moisture data are available, the PDSI is significantly correlated ($r = 0.5$ to 0.7) with observed soil moisture content within the top 1-m depth during warm-season months. The strongest correlation is in late summer and autumn, and the weakest correlation is in spring, when snowmelt plays an important role. Basin-averaged annual PDSI covary closely ($r = 0.6$ to 0.8) with streamflow for seven of world's largest rivers and several smaller rivers examined. The results suggest that the PDSI is a good proxy of both surface moisture conditions and streamflow. An empirical orthogonal function (EOF) analysis of the PDSI reveals a fairly linear trend resulting from trends in precipitation and surface temperature and an El Niño–Southern Oscillation (ENSO)-induced mode of mostly interannual variations as the two leading patterns. The global very dry areas, defined as PDSI < -3.0, have more than doubled since the 1970s, with a large jump in the early 1980s due to an ENSO-induced precipitation decrease and a subsequent expansion primarily due to surface warming, while global very wet areas (PDSI $> +3.0$) declined slightly during the 1980s. Together, the global land areas in either very dry or very wet conditions have increased from ~20% to 38% since 1972, with surface warming as the primary cause after the mid-1980s. These results provide observational evidence for the increasing risk of droughts as anthropogenic global warming progresses and produces both increased temperatures and increased drying.

1. Introduction

Droughts and floods are extreme climate events that percentage-wise are likely to change more rapidly than the mean climate (Trenberth et al. 2003). Because they are among the world's costliest natural disasters and affect a very large number of people each year (Wilhite 2000), it is important to monitor them and understand and perhaps predict their variability. The potential for large increases in these extreme climate events under global warming is of particular concern (Trenberth et al. 2004). However, the precise quantification of droughts and wet spells is difficult because there are many different definitions for these extreme events (e.g., meteorological, hydrological, and agricultural droughts; see Wilhite 2000 and Keyantash and Dracup 2002) and the criteria for determining the start and end of a drought or wet spell also vary. Furthermore, historical records of direct measurements of the dryness and wetness of the ground, such as soil moisture content (Robock et al. 2000), are sparse. In order to monitor droughts and wet spells and to study their variability, numerous specialized indices have been devised using readily available data such as precipitation and temperature (Heim 2000; Keyantash and Dracup 2002).

The Palmer Drought Severity Index (PDSI) is the most prominent index of *meteorological drought* used in the United States (Heim 2002). The PDSI was created by Palmer (1965) with the intent to measure the cumulative departure (relative to local mean conditions) in atmospheric moisture supply and demand at the surface. It incorporates antecedent precipitation, moisture supply, and moisture demand [based on the classic work of Thornthwaite (1948)] into a hydrological accounting system. Palmer used a two-layer bucket-type model for soil moisture computations and made certain assumptions relating to field water-holding capacity and transfer of moisture to and from the layers based on limited data from the central United States (Palmer 1965; Heim 2002). The Palmer model also computes, as an intermediate term in the computation of the PDSI, the Palmer moisture anomaly index (*Z* index), which is a measure of surface moisture anomaly for the current month without the consideration of the antecedent conditions that

* The National Center for Atmospheric Research is sponsored by the National Science Foundation.

Corresponding author address: A. Dai, National Center for Atmospheric Research, P.O. Box 3000, Boulder, CO 80307-3000.
E-mail: adai@ucar.edu

characterize the PDSI. The Z index can track agricultural drought, as it responds quickly to changes in soil moisture (Karl 1986). The Z index relates to the PDSI through the following equation (Palmer 1965, p. 22): PDSI (m) = PDSI $\{m - 1 + [Z(m)/3 - 0.103$ PDSI $(m - 1)]\}$, where m is a month index. A detailed description of the Palmer model is given in Palmer (1965), Alley (1984), and Karl (1986).

Theoretically, the PDSI is a standardized measure, ranging from about −10 (dry) to +10 (wet), of surface moisture conditions that allows comparisons across regions and time. Guttman et al. (1992) found, however, that the normal climate conditions tend to yield more severe PDSI in the Great Plains than in other U.S. regions. The PDSI is also imprecise in its treatment of all precipitation as immediately available rainfall (i.e., no snow accumulation on the ground), the effects of vegetation on surface evapotranspiration, the calibration coefficients (Karl 1986), and some other processes (Alley 1984). For example, Palmer assumed that evapotranspiration occurs at the potential rate (i.e., according to Thornthwaite 1948) from the top soil layer until all the available moisture in this layer has been depleted. Only then can moisture be removed from the underlying layer of soil. Although these assumptions are not unreasonable, they are only crude approximations even for bare soil surfaces (Philip 1957). Other factors such as changes in surface solar radiation due to changes in cloudiness or aerosol concentrations (Abakumova et al. 1996; Liepert 2002) are not considered explicitly in the Palmer model, although the effect of solar radiation is implicitly considered through surface temperature. Also, the PDSI cannot reflect soil moisture conditions when the soil is frozen, or when snow accumulation and melt are a significant factor, such as during the winter and spring months at mid- and high latitudes. Nevertheless, the PDSI is still an approximate measure of the cumulative effect of *atmospheric* moisture supply and demand (i.e., meteorological droughts) in these situations. We emphasize that, by design, the PDSI is not always a good measure of soil moisture and thus agricultural droughts, although we show that the PDSI does correlate with soil moisture content during warm seasons.

On the positive side, the PDSI uses both precipitation and surface air temperature as input, in contrast to many other drought indices that are based on precipitation alone (Keyantash and Dracup 2002). This allows the PDSI to account for the basic effect of surface warming, as has occurred during the twentieth century, on droughts and wet spells. The effect of surface temperature, which accounts for 10%–30% of PDSI's variance, comes through the potential evapotranspiration, which was computed from Thornthwaite's (1948) formula in the Palmer model and used as a measure of the atmospheric demand for moisture. As precipitation and surface air temperature are the only two climate variables with long historical records, the PDSI makes full use of these data and can be readily calculated for the last hundred years or so for most land areas.

Besides its routine use for monitoring droughts in the United States, the PDSI has been used to study drought climatology and variability in the United States (e.g., Karl and Koscielny 1982; Karl 1986), Europe (Domonkos et al. 2001; Lloyd-Hughes and Saunders 2002), Africa (Ntale and Gan 2003), Brazil (dos Santos and Pereira 1999), and other areas. The PDSI was also used in tree-ring-based reconstructions of droughts in the United States (e.g., Cole and Cook 1998; Cook et al. 1999; Fye et al. 2003). Most of these studies are regional and focus on a particular location or nation. One exception is Dai et al. (1998) who calculated the PDSI for global land areas for 1900–95 and analyzed the influence of El Niño–Southern Oscillation (ENSO) on dry and wet areas around the globe. This study updates the global PDSI dataset of Dai et al. (1998), provides a detailed evaluation of the PDSI against available soil moisture and streamflow data, examines the trends and leading modes of variability in the twentieth-century PDSI fields, and investigates the impact of surface warming of the latter half of the twentieth century on global drought and wet areas. The global PDSI dataset (available from http://www.cgd.ucar.edu/cas/catalog/climind/pdsi.html) has been used by a number of groups and will be updated periodically in the future. We emphasize that the PDSI is better used on annual time scales and should not be used as a measure of soil moisture content during cold seasons at high latitudes. In addition, quantitative interpretations of dryness or wetness for a given PDSI value depend on local mean climate conditions. For example, a PDSI value of +4 may imply floods in the central United States, but only moderate rainfall (by central U.S. standards) in northern Africa.

2. Datasets and procedures

Table 1 lists the datasets used in this study. To calculate the monthly PDSI, we used the Climate Research Unit (CRU) surface air temperature data (Jones and Moberg 2003; regridded to 2.5° × 2.5° grid). Precipitation data for 1948–2003 were obtained from the National Centers for Environmental Prediction (NCEP) Climate Prediction Center (Chen et al. 2002) and were created by gridding data from about 5000 to 16 500 gauges during 1948–97 and about 3500 gauges for more recent years using the optimal interpolation scheme; for the pre-1948 period, we used the precipitation data from Dai et al. (1997). The monthly anomalies of Dai et al. (1997) were adjusted to have zero mean values for 1950–79 and then added to the 1950–79 mean of Chen et al. (2002) to obtain the total precipitation used for the PDSI calculation. For field water-holding capacity (*awc*), we used a soil texture–based water-holding-capacity map from Webb et al. (1993). If *awc* is no more than 2.54 cm (or 1 in.), then *awc* is assigned to the top soil layer, and the bottom layer has zero capacity, oth-

TABLE 1. Datasets used in this study. All are monthly.

Variables	Type and coverage	Resolution	Period	Source and reference
P	Rain gauge, land	2.5° × 2.5°	1850–2003	Dai et al. (1997); Chen et al. (2002)
T	Surface obs, land	5° × 5°	1851–2003	CRUTEM2; Jones and Moberg (2003)
Streamflow	Station, land		1–100+ yr	NCAR; Dai and Trenberth 2002
Soil moisture	Station, land		10–21 yr	Robock et al. (2000)
	Illinois	19 stations	1981–2001	Hollinger and Isard (1994)
	China	43 stations	1981–91	Robock et al. (2000)
	Mongolia	42 stations	1978–93	Robock et al. (2000)
	Former USSR	50 stations	1972–85	Vinnikov and Yeserkepova (1991)
Soil water-holding capacity	Derived, land	1° × 1°	climatology	Webb et al. (1993)

erwise, the top layer has 2.54-cm water-holding capacity while the bottom layer has (*awc* − 2.54)-cm capacity. The temperature and precipitation data likely contain some errors; however, various data quality controls were done to minimize data inhomogeneities by previous analyses (e.g., Jones and Moberg 2003; Dai et al. 1997; Chen et al. 2002), and the time series are thought to be reliable over most land areas. The relatively low resolution (2.5° × 2.5°) used here does not resolve small-scale variations such as those over mountains.

The PDSI has often been used without rigorous evaluation as it is not directly comparable to any measured variables, such as soil moisture content and streamflow. Soil moisture content reflects the amount of precipitation retained locally after runoff. This depends on many factors, including field water-holding capacity (a function of soil texture and depth), antecedent soil conditions, and precipitation frequency and intensity (Trenberth et al. 2003). For example, a severe thunderstorm can create a lot of surface runoff or even flash floods, but may leave the subsurface soil still dry. In contrast, hours of light, stratiform rain can moisten the soil thoroughly with little runoff. Furthermore, surface and subsurface runoff may take weeks to months to reach the downstream part of the world's major rivers. These situations illustrate the complex relationships among local atmospheric moisture supply and demand (based on which the PDSI is computed), soil moisture, and runoff or streamflow. Nevertheless, on regional and river-basin scales and averaged annually, the PDSI, soil moisture, and streamflow should correlate with each other, as these all are measures of large-scale droughts and wet spells that are driven by regional atmospheric moisture supply (i.e., precipitation) and demand (i.e., evapotranspiration). Dai et al. (1998) showed that area-averaged PDSI is significantly correlated ($r = 0.63 - 0.75$) with streamflow of the twentieth century over the United States, midlatitude Canada, Europe, and southeast Australia. Here, we compare the PDSI with available soil moisture data obtained from the Global Soil Moisture Data Bank (http://climate.envsci.rutgers.edu/soil_moisture/) (Robock et al. 2000) over Illinois, Mongolia, and parts of China and the former Soviet Union (fUSSR). The soil moisture stations [see Robock et al. (2000) for their locations] were grouped into regions defined by latitudes and longitudes to facilitate comparisons with the gridded PDSI values. Nearby stations were averaged first and then combined with other stations to obtain the arithmetical mean for the region. We also integrate the PDSI over a number of large river basins for comparison with observed river flow (from Dai and Trenberth 2002) during the twentieth century. In this comparison, we focus on the annual time series, ignoring the time lag between local runoff and downstream river flows. Significant correlations between the PDSI and the other drought measures should provide further support of the usefulness of the PDSI dataset.

3. PDSI versus soil moisture

Figure 1 compares the observed and Palmer model–calculated soil moisture content for Illinois. For the summer half year, the Palmer model captures both the mean seasonal and year-to-year variations in the top 0.9-m depth very well with only small biases. This is remarkable considering that the Palmer model is very simple compared to modern land surface models (e.g., Dai et al. 2003) and was driven by only monthly temperature and precipitation. The largest bias, which does not affect correlation, is in September when the calculated mean soil moisture is lower and interannual anomalies are larger than observed. Correlations between the calculated total moisture content and the observed moisture content at each depth are strongest and significant up to ~1.25 m depth in September, insignificant during March–April, and significant up to only ~0.5 m depth during May–June (Fig. 1c). The low correlation during spring is not surprising as snowmelt is not considered in the simple Palmer model but has large effects on soil moisture in Illinois. The snow effects gradually diminish during May–June, and soil moisture is increasingly affected by monthly rainfall so that the Palmer model performs better. Furthermore, Fig. 1b suggests that soil moisture anomalies in the Palmer model and the data have different lower bounds.

Significant correlations are also found between the observed soil moisture content and the PDSI for Illinois (Fig. 2). The interannual correlation (Fig. 2a) is reduced considerably by the three lower-right points, and the correlation at depths is lower than that shown in Fig. 1c except for May when the PDSI actually correlates strongest with the observed soil moisture. This May

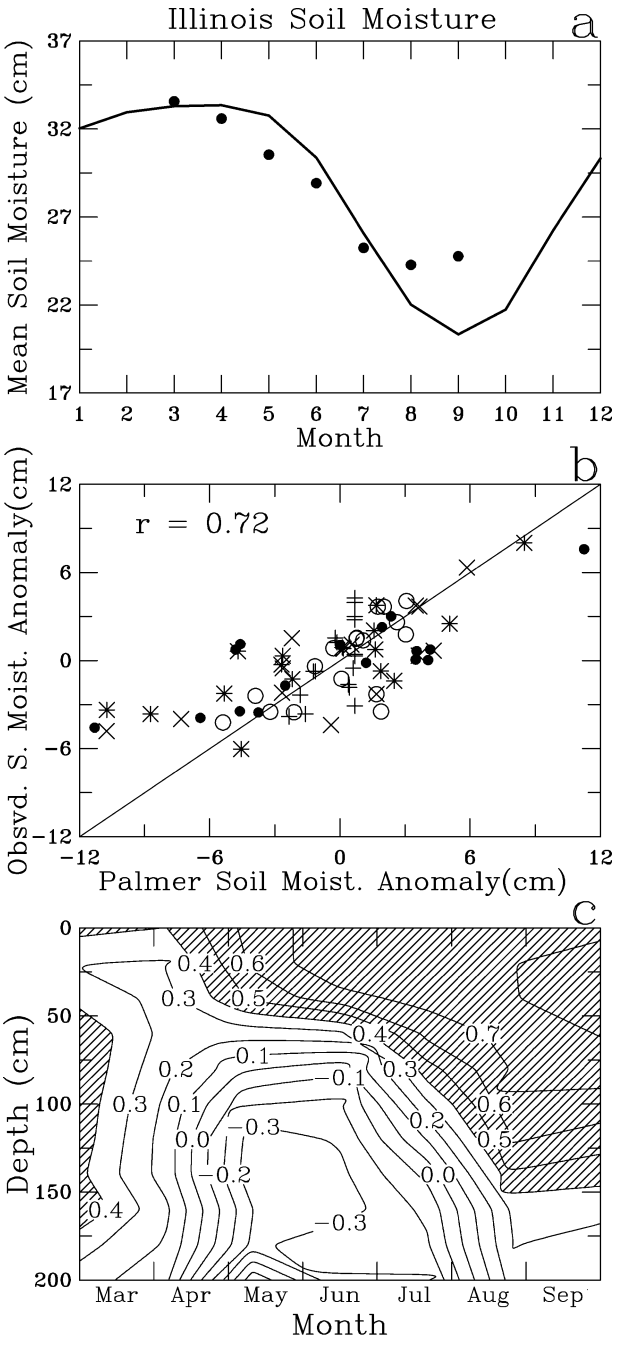

FIG. 1. (a) Mean annual cycle of Palmer model–calculated (solid line) and observed (dots, for top 0.9-m depth, 17 stations) soil moisture content for Illinois. (b) Scatterplot of monthly anomalies of soil moisture from the Palmer model and observations for Illinois during 1981–2001. Here r is the correlation coefficient of all the data points. Legend: symbols +, ○, ×, *, and ● are, respectively, for months 5, 6, 7, 8, and 9. (c) Distribution of the correlation coefficient between the Palmer and observed soil moisture as a function of month and soil depth. Values below ~0.4 are statistically insignificant. There are insufficient soil moisture data for months Oct–Feb.

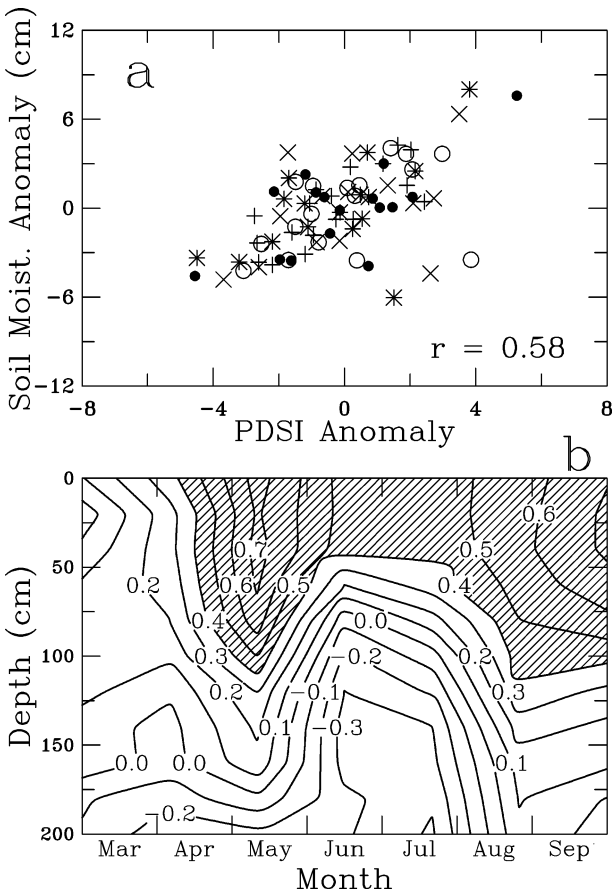

FIG. 2. (a) Scatterplot of monthly anomalies of the PDSI and observed soil moisture within top 0.9-m depth for Illinois during 1981–2001. Here r is the correlation coefficient of all the data points. Legend: symbols +, ○, ×, *, and ● are, respectively, for months 5, 6, 7, 8, and 9. (b) Distribution of the correlation coefficient between the PDSI and observed soil moisture as a function of month and soil depth. Values below ~0.4 are statistically insignificant. There are insufficient soil moisture data for months Oct–Feb.

maximum is a bit surprising given the snow effect discussed above.

The Palmer model–calculated soil moisture content has large biases for many of the regions in China, Mongolia, and fUSSR, as the model was tuned to conditions typical for the central United States. On the other hand, the PDSI and Z index are standardized indices that have near-zero biases. As such, we compare the PDSI and Z with observed soil moisture content outside the United States.

Table 2 shows the correlation coefficients between the observed monthly mean soil moisture content (in top 1-m depth, except Illinois where it is top 0.9 m) and the Palmer model–calculated soil moisture content, Z index, PDSI, and observed precipitation for regions where soil moisture data are available (from Robock et al. 2000). The scatterplots of the PDSI versus observed soil moisture (SM) content for the Chinese and fUSSR regions are shown in Figs. 3 and 4, respectively. We

TABLE 2. Correlation coefficients of monthly anomalies of observed SM content (top ~1 m depth) vs Palmer model–calculated soil moisture (PSM), moisture anomaly index (*Z*), PDSI, and observed precipitation (P) over regions where soil moisture data are available. Boldface numbers are statistically significant at the 5% level. See Table 1 for data periods.

Region (No. of stations)	SM vs PSM	SM vs *Z*	SM vs PDSI	SM vs P	Months included
Illinois (17)	**0.72**	**0.72**	**0.58**	**0.64**	May–Sep
Northeast China (14) (40°–47.5°N, 122.5°–132.5°E)	**0.50**	0.24	**0.50**	0.16	May–Oct
East China (7) (32.5°–35°N, 110°–120°E)	**0.58**	**0.51**	**0.63**	**0.39**	Mar–Dec
North-central China (5) (35°–42.5°N, 105°–110°E)	**0.44**	0.33	**0.61**	0.31	May–Aug
South China (3) (22.5°–25°N, 102.5°–110°E)	**0.45**	**0.36**	**0.55**	0.23	Jan–Dec
West Mongolia (7) (45°–50°N, 90°–97.5°E)	**0.44**	**0.49**	**0.50**	**0.42**	Jun–Oct
Central Mongolia (25) (45°–50°N, 97.5°–107.5°E)	**0.42**	**0.33**	**0.52**	**0.33**	May–Sep
East Mongolia (6) (45°–50°N, 110°–115°E)	0.29	**0.40**	**0.48**	**0.38**	May–Sep
fUSSR box 1 (11) (50°–55°N, 70°–100°E)	**0.45**	**0.42**	**0.54**	**0.34**	Apr–Oct
fUSSR box 2 (14) (47.5°–55°N, 45°–60°E)	**0.67**	**0.59**	**0.69**	**0.45**	May–Nov
fUSSR box 3 (8) (50°–60°N, 27.5°–40°E)	**0.77**	**0.57**	**0.71**	**0.38**	Apr–Nov
fUSSR box 4 (9) (42.5°–47.5°N, 52.5°–77.5°E)	**0.42**	**0.58**	**0.50**	**0.57**	Apr–Jul

excluded most winter and spring months from the correlation since there were either insufficient moisture data or because snow interferes with the relationships with the PDSI and *Z* index during these months, except for South China where it rarely snows. In these comparisons of monthly data, we consider only simultaneous correlations. Table 2 and Figs. 2 and 4 show that the PDSI is more consistently correlated with the observed SM than are the modeled SM, *Z* index, and observed precipitation. The observed SM versus PDSI correlation coefficients range from ~0.5 to 0.7, whereas the correlation with the *Z* index and precipitation are generally lower, as the *Z* index and precipitation time series have more high-frequency variations than the PDSI. The modeled SM correlates with the SM data better than the *Z* index, but it can have large mean biases outside the central United States, as the Palmer model was tuned to central U.S. conditions. Figures 2a, 3, and 4 show that the quantitative relationship (i.e., the slope) between the observed SM and PDSI does not vary significantly with month over most of the regions, except for east China where October–December PDSI varies more with SM than in other months.

As stated in sections 1 and 2, the Palmer model does not deal with snow and some other processes affecting soil moisture content. The PDSI was not designed to be and should not be considered a direct measure of soil moisture content. Therefore, one should not expect a perfect correlation between the two. In addition, the soil moisture data, which have only two–three measurements per month and contain many missing values, likely have large temporal and spatial sampling errors, especially for regions with a small number of stations such as South China and west Mongolia (Table 2). These errors also contribute to the scatter in Figs. 1b, 2a, 3, and 4. The records of the soil moisture data outside the United States are relatively short so that the SM versus PDSI correlation at each depth and for each month are noisy (not shown); nevertheless, the PDSI was found to correlate with the SM up to 1-m depth in most of the regions.

4. PDSI versus river flow

The time series of annual streamflow rates and basin-averaged PDSI for world's largest 10 rivers (except No. 5 Brahmaputra and No. 10 Mekong, both in southern Asia, whose streamflow records are too short), plus 4 smaller rivers that have long records are compared (Fig. 5). In deriving the basin-averaged PDSI, we required that more than half of the basin areas had data. This mostly affects the PDSI of the earlier years of the time series. Figure 5 shows that the basin-averaged PDSI covaries with streamflow rates for all of the 12 rivers except for the Yenisey. For example, the PDSI over the Amazon basin closely follows the flow rates at Obidos during the last three decades, it suggests low flow rates in the 1960s and near-normal flows in the 1950s when there were no streamflow data, and it matches the measured flow rates in the 1940s. For the Orinoco, Mississippi, and Paraná, both the PDSI and streamflow show some increases after the late 1950s, or early 1960s for Paraná. For the Congo basin, large increases occurred around 1960 in both the PDSI and steamflow; thereafter, they both decreased gradually. Even over smaller river basins such as the Columbia in the western United States

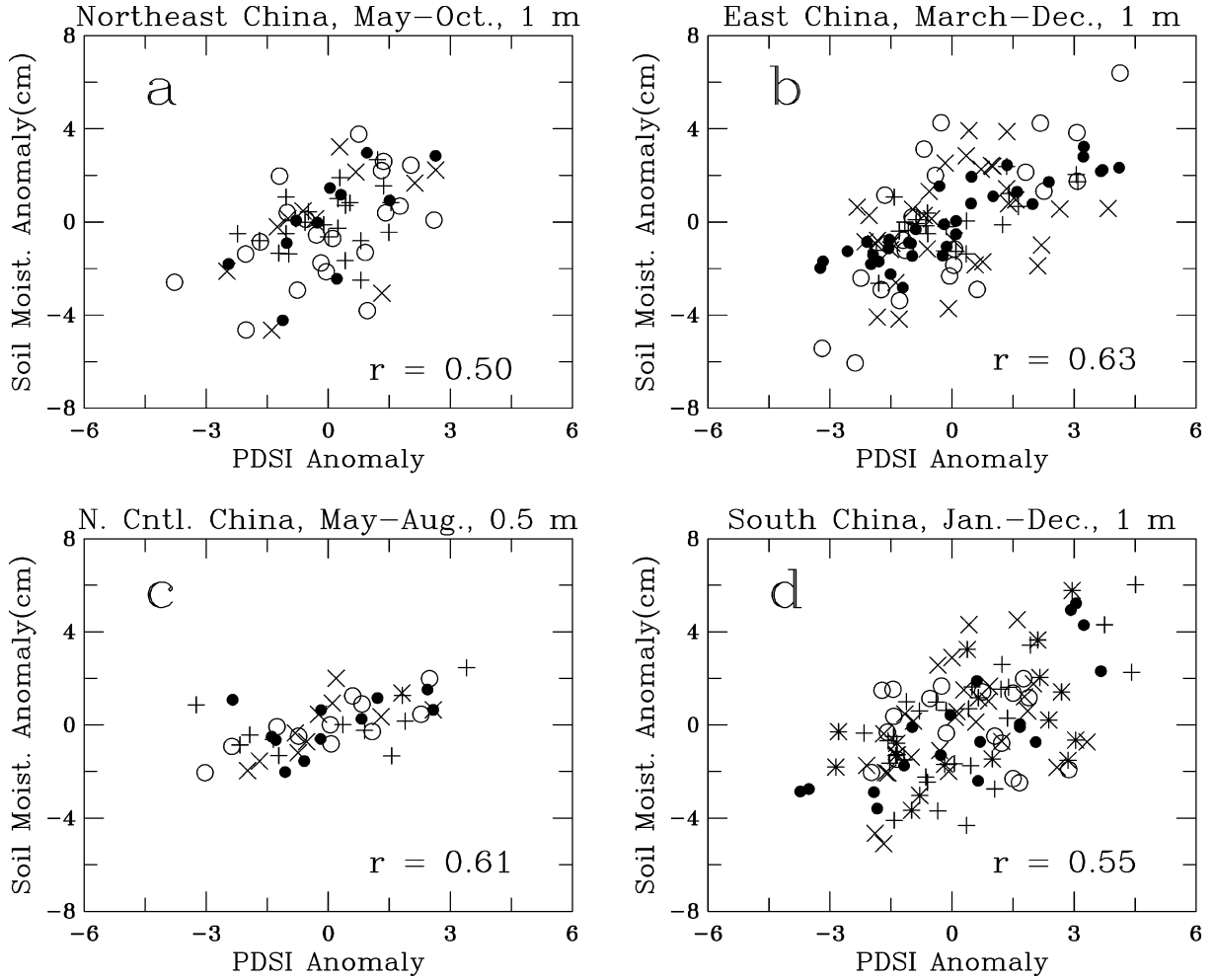

FIG. 3. Scatterplots of monthly anomalies of PDSI vs observed soil moisture content within top 1-m [except (c), which is for top 0.5 m] depth within China during 1981–91. Here r is the correlation coefficient of all the data points. (a) Northeast China (14 soil moisture stations), (b) east China (7 stations), (c) north-central China (5 stations), and (d) south China (3 stations). Legend: symbols +, ○, ×, and ● are, respectively, for months 6, 7–8, 9, and 10 in (a), 3–4, 5–6, 7–9, and 10–12 in (b), and 5, 6, 7, and 8 in (c); symbols +, ○, ×, *, and ● are, respectively, for months 1–3, 4–5, 6–8, 9–10, and 11–12 in (d).

and Canada, Susquehanna in the northeast United States, and Göta in Sweden, the PDSI and streamflow covary closely (Fig. 5); both show large multiyear variations and rapid switches of dry and wet decades (e.g., ~1969 for Göta, ~1945 for Columbia). For most rivers, the correlation coefficient between the observed annual streamflow and basin-averaged annual PDSI is comparable to that between the streamflow and basin-averaged precipitation (from previous winter to autumn of the year for river basins with significant snowmelt). The reason that annual PDSI correlates with annual river flows even for river basins with large snowmelt, such as the Lena and Columbia, is that winter and spring snowfall increases the PDSI during these and subsequent months, leading to correlations on annual time scales.

The low correlation between the PDSI and streamflow over the Yenisey basin results largely from their opposite trends during 1960–2000, when precipitation changed little while temperature increased by ~2°C over this basin (not shown). The decreasing PDSI trend over the Yenisey basin is caused by the large warming over the region. Rain gauges are relatively sparse over the Yenisey basin (Chen et al. 2002), which may contribute to the low correlation between the streamflow and basin-averaged precipitation ($r = 0.24$). Withdrawal of water for industrial and agricultural use should decrease the river flow while large dams should mostly alter its annual cycle (Yang et al. 2004); they cannot explain the upward trend in Yenisey's flow rates since the 1960s (Fig. 5).

5. Leading patterns in global PDSI

Figure 6 shows temporal and spatial patterns of the two leading empirical orthogonal functions (EOFs) of

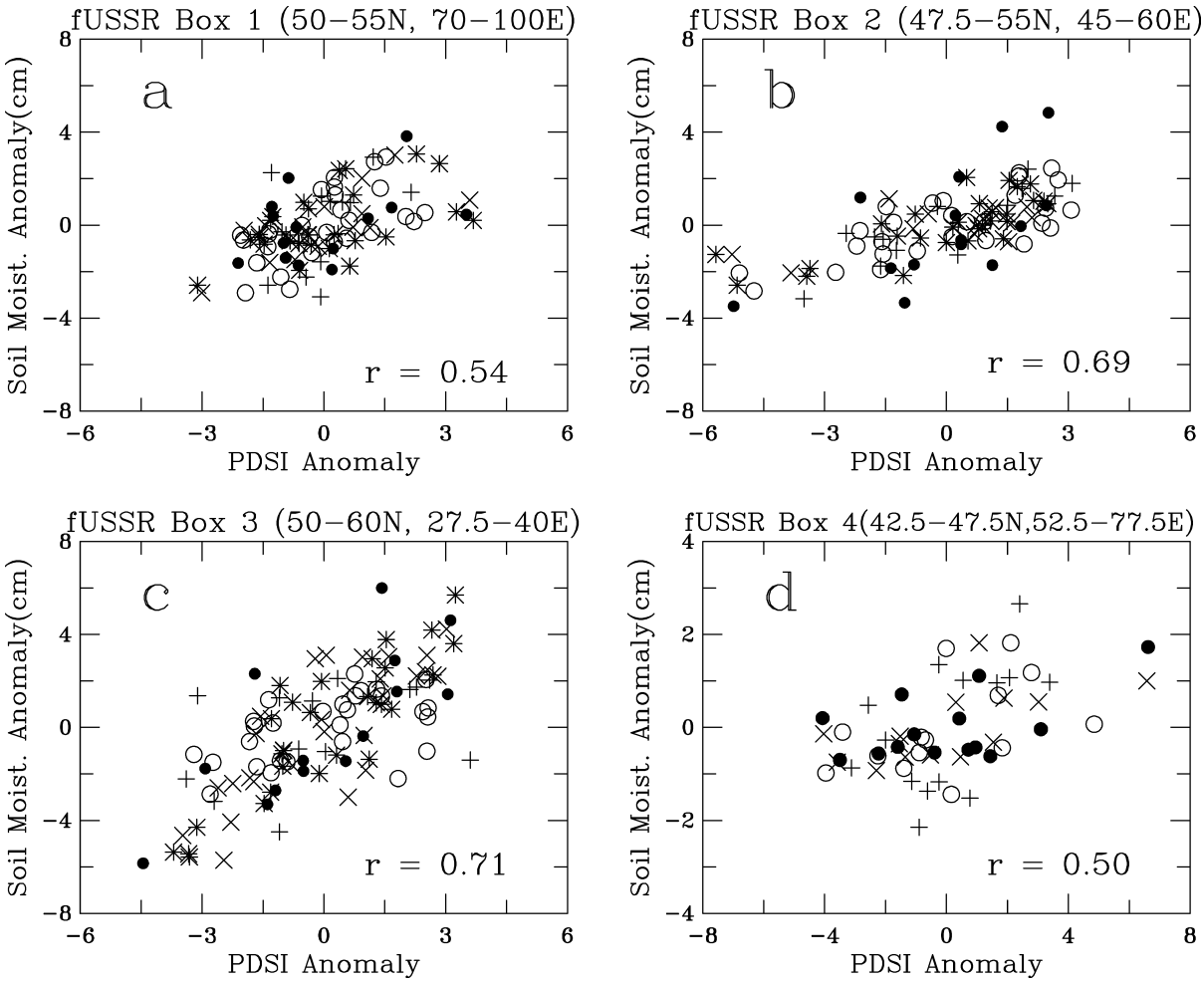

FIG. 4. Same as Fig. 3, but for the period 1972–85 and over four regions of the former Soviet Union: (a) 50°–55°N, 70°–100°E, 11 soil moisture stations; (b) 47.5°–55°N, 45°–60°E, 14 stations; (c) 50°–60°N, 27.5°–40°E, 8 stations; and (d) 42.5°–47.5°N, 52.5°–77.5°E, 9 stations. Legend: symbols +, ○, ×, *, and ● are, respectively, for months 4, 5–6, 7, 8–9, and 10 in (a), 5, 6–7, 8, 9–10, and 11 in (b), and 4, 5–6, 7–8, 9–10, and 11 in (c), symbols +, ○, ×, *, and ● are, respectively, for months 4, 5, 6, and 7 in (d).

the correlation matrix of monthly PDSI from 1900 to 2002. Almost all land boxes except Greenland and Antarctica have data after about 1948, and this meets the minimum of 50 yr of data for each box we required for the EOF analysis. The percentages of variance explained by the EOFs are comparable to those of leading EOFs of land precipitation (Dai et al. 1997). The principal component time series of the first EOF represents a linear trend and suggests drying over the red areas, such as northern and southern Africa, the Middle East, Mongolia, and eastern Australia, and wetting over the blue areas, such as the United States, Argentina, and parts of Eurasia. Dai et al. (1997) showed an EOF with linear increasing trends in global land precipitation during 1900–88, with large increases over the United States, Argentina, and much of Eurasia. The moistening effect of the precipitation increases was modulated by the drying effect of surface warming over many regions during the twentieth century, resulting in regional drying and wetting shown by the PDSI EOF 1. This is in contrast to spatially uniform increases in the precipitation trend EOF (Dai et al. 1997). We further examine the PDSI trends in section 6.

The second EOF (Fig. 6) of the PDSI reveals temporal and spatial patterns that are highly correlated with ENSO, suggesting that this pattern of mostly multiyear variability is ENSO related and hence represents a true mode of climate system behavior. This mode is induced mainly by the precipitation anomalies associated with ENSO (e.g., Ropelewski and Halpert 1987; Dai and Wigley 2000; Trenberth and Caron 2000), as shown by the strong similarity between the ENSO EOFs of the PDSI and land precipitation (Dai et al. 1997), while the effects of ENSO-induced temperature anomalies (Kiladis and Diaz 1989) are small. Lag correlations (Fig. 6) suggest that the maximum influence of ENSO on land surface conditions lags the ENSO index in the tropical Pacific by about 6 months. This time lag results partly

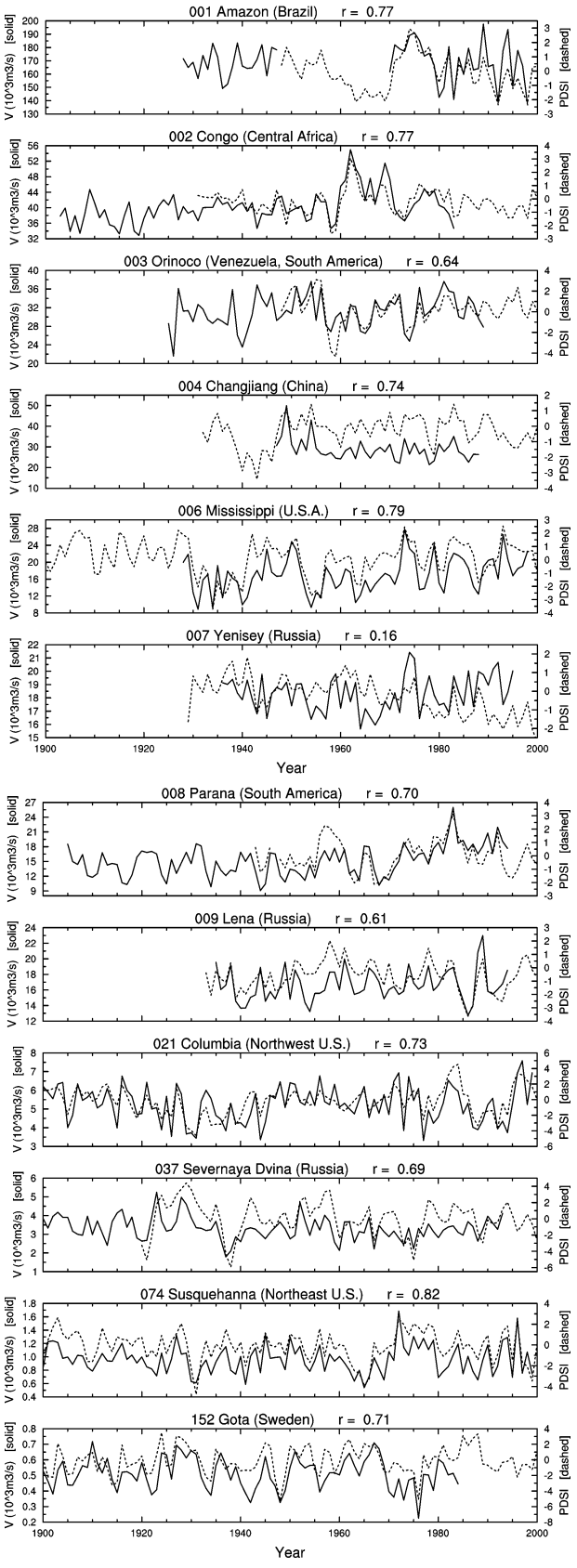

from the considerable memory of soil moisture. The ENSO EOF shows that during the typical warm phase (El Niño) of ENSO, surface conditions are wetter than normal in much of North America except Alaska, Europe, central Asia, and southern South America, but drier than normal in eastern Australia, northern South America, and southern Asia, areas known to experience droughts during El Niños. During the typical cold phase (La Niña) of ENSO, these anomalies reverse sign. This linear result is only a first-order approximation, as asymmetry exists between the cold and warm phases (e.g., Monahan and Dai 2004).

6. Trends in PDSI, and global dry and wet areas

The top and middle panels of Fig. 7 show the linear PDSI trends during 1900–49 and 1950–2002 calculated using all monthly data. During the first half of the twentieth century, the Guinea Coast, southern Africa, parts of Canada, and southern and central Europe became drier, while it became wetter in most of Asia, Alaska, and parts of South America as precipitation increased over these regions while surface warming was relatively small (not shown). Since 1950, substantial increases of precipitation (not shown) have occurred in Argentina, the southern United States, and most of western Australia, which resulted in wetter conditions in these regions (Fig. 7). However, most parts of Eurasia, Africa, Canada, Alaska, and eastern Australia became drier from 1950 to 2002. Large surface warming has occurred since 1950 over these regions (Fig. 8), which is a major cause for the widespread drying over these regions. Without the warming, the PDSI decreases would have been much smaller and less pervasive, as shown by the bottom panel of Fig. 7. In fact, the warming by the end of the twentieth century results in decreases of 0.5–1.5 of PDSI over most land areas (Fig. 8). These decreases are very significant considering that a PDSI of less than −0.5 is classified as dry or drought conditions by Palmer (1965). The largest drying effect occurred over central Asia and Canada, where the surface air has warmed 1.5°–2.0°C since 1950 (Fig. 8). The drying over the arid Middle East and Sahel is also large after 1950, with contributions from both decreased precipitation and increased temperature over the regions (Figs. 7 and 8).

We examined PDSI trends in winter and summer months and found only small differences, even though surface warming during 1950–2002 over the northern mid- and high-latitude land areas was much larger in winter than summer (1.5°–4.0° versus 0.5°–1.5°C).

←

FIG. 5. Basin-averaged annual PDSI (dashed) compared with observed annual river-flow rates (V, 10^3 m^3 s^{-1}, solid line) at the farthest downstream station (from Dai and Trenberth 2002) for world's largest 10 rivers (except No. 5 Brahmaputra and No. 10 Mekong, whose records are too short) and 4 smaller rivers that have long records of streamflow.

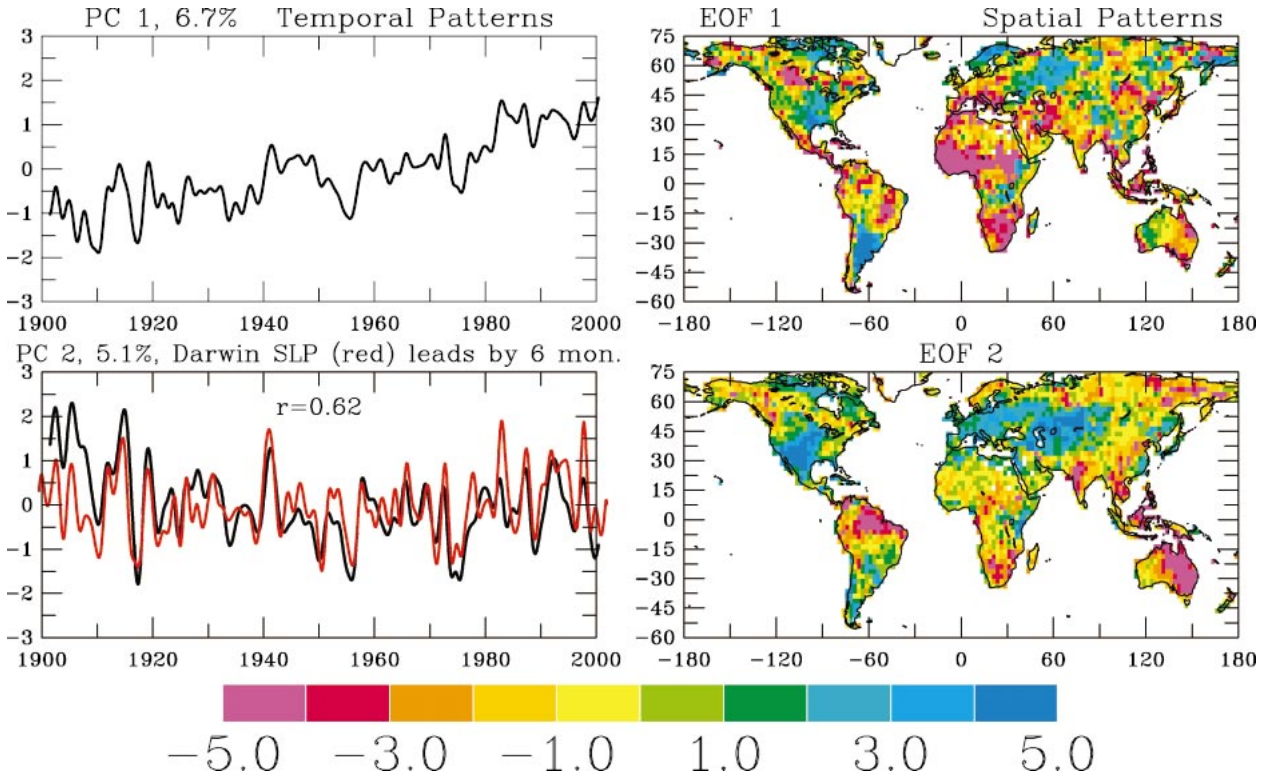

FIG. 6. (left) Temporal (black) and (right) spatial patterns of the two leading EOFs of the monthly PDSI (normalized by its standard deviation prior to the EOF analysis). Red (blue) areas are dry (wet) for a positive temporal coefficient. Also shown in the lower-left panel (red) is the Darwin mean sea level pressure shifted to the right by 6 months to obtain the maximum correlation ($r = 0.62$). Variations on <2 yr time scales were filtered out in the left panels. The percentage variance explained is shown on the top of the left panels.

There are two reasons for this. First, for a given increase of surface temperature, the potential evapotranspiration (i.e., atmospheric moisture demand) increases much more in summer than in winter because of the nonlinear dependence of the saturation vapor pressure on temperature. Second, the PDSI has a fairly long memory, partly reflecting the memory of soil moisture, so that surface warming in winter and spring can still affect summer PDSI.

After 1950, PDSI values are available for almost all land boxes except Antarctica and Greenland. This allows us to reliably estimate the percentage areas in very dry or, in Palmer's (1965) classification, ''severe'' or ''extreme'' drought (PDSI < -3.0), very wet (PDSI $> +3.0$), and in either very dry or very wet conditions for 1950–2002. Figure 9 shows that the very dry area has more than doubled (from ~12% to 30%) since the 1970s, with a large jump in the early 1980s due to precipitation decreases and subsequent expansion primarily due to surface warming. The precipitation decreases around the early 1980s that occurred mainly over ENSO-sensitive regions such as the Sahel, southern Africa, and east Asia as El Niños, which reduce rainfall over these regions (Dai et al. 1997; Dai and Wigley 2000), became more prominent after the late 1970s (Trenberth and Hoar 1996). In contrast, the warming-induced drying has occurred over most land areas, with the largest effects in northern mid- and high latitudes (Fig. 8). Coinciding with increases in the very dry areas from the early 1980s to early 1990s, the global very wet land areas declined by ~5%, with precipitation as the major contributor during the early 1980s and temperature more important thereafter. Together, the global areas under either very dry or very wet conditions decreased slightly by ~7% from 1950 to 1972, with precipitation as the primary contributor. Since 1972, the dry plus wet percentage areas have increased from ~20% to 38% (a 90% increase), with surface warming as the primary cause after the middle 1980s (Fig. 9).

The changes in the very dry and very wet areas vary with region (Fig. 10). For example, over the contiguous United States, recent precipitation increases (Karl and Knight 1998; Groisman et al. 2004) resulted in increased wet areas after 1970, whereas the very dry areas were doubled during the ''Dust Bowl'' era in the 1930s, and since the middle 1980s have stayed above normal. A steady, upward trend in the dry plus wet areas is evident over the United States since the 1970s (Fig. 10). Over western Europe (west of 30°E), the very wet areas were relatively stable during the last 50 yr while the very dry areas have increased substantially since the 1970s (Fig. 10). In Australia, large interannual variations in the wet

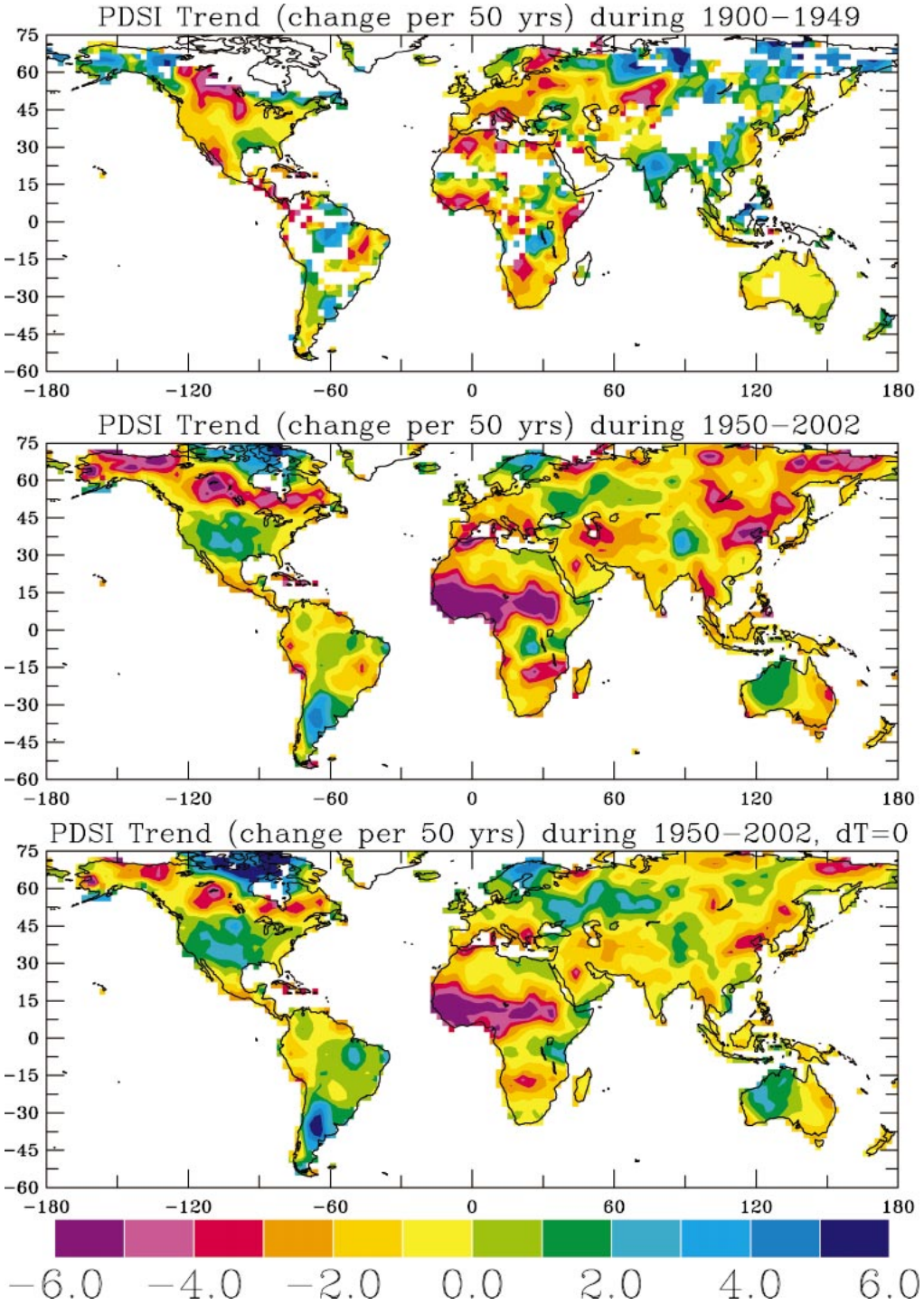

FIG. 7. Maps of linear trends of PDSI [change (50 yr)$^{-1}$, calculated with both precipitation and temperature changes] during (top) 1900–49 and (middle) 1950–2002. (bottom) The trends of PDSI calculated without temperature changes. Red (blue) areas indicate drying (wetting).

and dry areas are associated with ENSO events (e.g., in 1965/66 and 1982/83), while secular trends are small on the continental scale (Fig. 10), although the ENSO-related 2002/03 drought is perhaps the worst on record and its severity has been partly attributed to the warming trend (Nicholls 2004). ENSO influences on the dry and wet areas are also large over the Sahel (11–18°N, 18°W–10°E) and southern Africa (south of 15°S), both of which

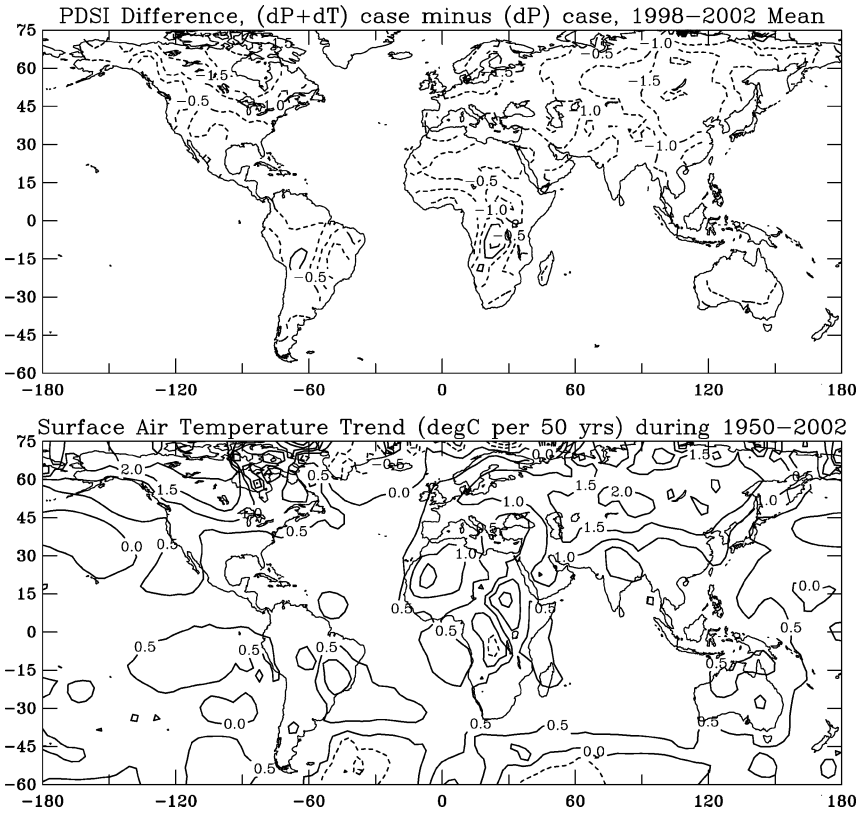

FIG. 8. (top) The 1998–2002 mean difference of the PDSI calculated with and without temperature changes. (bottom) Linear trends of observed surface air temperature [°C (50 yr)$^{-1}$] during 1950–2002. Dashed contours have negative values.

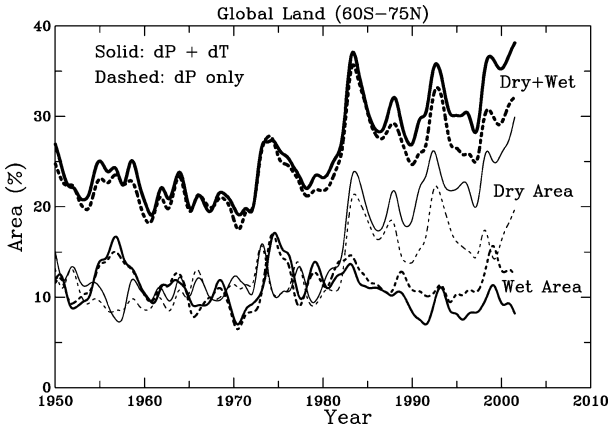

FIG. 9. Smoothed time series of the percentage of the total land areas within 60°S–75°N that were in very dry (PDSI < -3.0; thin lines), very wet (PDSI $> +3.0$; medium lines), and very dry or wet (thickest lines at the top) conditions from 1950 to 2002. The solid lines are based on the PDSI calculated with both precipitation and temperature changes, while the dashed lines are without temperature changes (i.e., due to precipitation alone).

have become considerably drier since the 1970s. This is also the case over eastern Asia (east of 90°E) where the very dry areas increased from ~10% in the 1970s to over 30% in 2000 (Fig. 10). In the Sahel, more than half of the areas are in drought conditions (PDSI $<$ -3.0) and there have been essentially no wet areas since the 1970s, consistent with analyses of Sahel rainfall data (e.g., Dai et al. 2004).

7. Summary and concluding remarks

We derived a monthly PDSI dataset for 1870–2002 using monthly precipitation and surface air temperature data for global land areas, except Antarctica and Greenland, on a 2.5° × 2.5° grid. The PDSI was compared with warm-season soil moisture data from Illinois and Eurasia and streamflow records for the world's largest rivers and some smaller rivers with long records. The effects of surface warming on dry and wet areas were investigated by comparing the PDSI cases with and without temperature changes.

The Palmer model simulates the seasonal and interannual variations of top 1-m soil moisture very well for Illinois, but has large biases for many regions in Eurasia. The PDSI variations are correlated ($r = 0.5 \sim 0.7$) with those in the observed soil moisture content within the

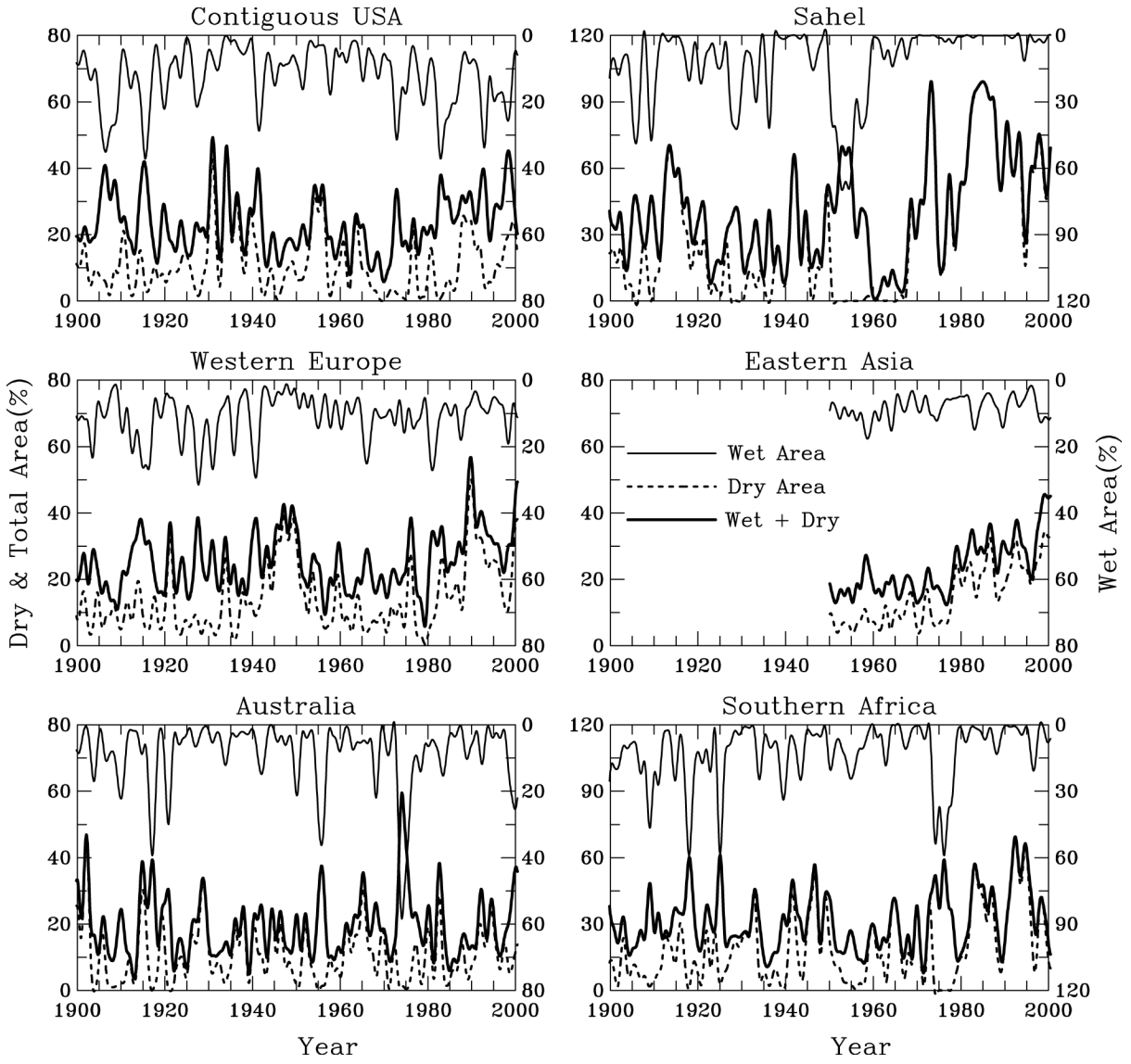

FIG. 10. Smoothed time series of percentage areas in very dry (PDSI < -3.0; dashed line), very wet (PDSI $> +3.0$; upper thin solid line), and the sum of the two (thick solid line) over the regions where data are sufficient during the plotted periods. Note that the very wet area is plotted using the downward scale on the right-hand-side ordinate (0%–80% except for the Sahel and southern Africa), and the dry and total areas are on the left-hand-side ordinate.

top 1-m depth during warm-season months, with the strongest correlation in late summer and autumn, and the weakest correlation in spring, as the Palmer model does not account for the effects of snow melting. The correlation with the soil moisture data is higher for the PDSI than precipitation, suggesting that the PDSI represents surface moisture conditions better than precipitation alone.

The river basin–averaged annual PDSI covary ($r = 0.6 \sim 0.8$) with annual streamflow for seven of the world's largest rivers and several smaller rivers examined and may be used as a proxy of annual-mean streamflow when the latter is unavailable. Both the PDSI and streamflow undergo rapid switches of dry and wet decades over some river basins such as the Congo, Columbia, and Göta. They also show upward trends during the last 40 yr or so for the Orinoco, Mississippi, and Paraná. Results suggest strong relations of the PDSI with both soil moisture and streamflow, partly reflecting the correlation on annual time scales between agricultural and hydrological droughts.

EOF analyses of the PDSI revealed a linear trend during 1900–2002 resulting from a combination of precipitation and surface temperature trends, with drying over northern and southern Africa, the Middle East, Mongolia, and eastern Australia, and moistening over the United States, Argentina, and parts of Eurasia. The second EOF of the PDSI reflects ENSO with a 6-month

time lag, resulting primarily from precipitation anomalies.

The PDSI trends of 1900–49 show that the Guinea Coast, southern Africa, parts of Canada, and southern and central Europe became drier, while it became wetter in most of Asia, Alaska, and parts of South America during the period. From 1950 to 2002, precipitation increases over Argentina, the southern United States, and most of western Australia resulted in wetter conditions (i.e., higher PDSI) in these regions. However, most of Eurasia, Africa, Canada, Alaska, and eastern Australia became drier from 1950 to 2002, partly because of large surface warming since 1950 over these regions.

The very dry areas (PDSI < -3.0) over global land have increased from ~12% to 30% since the 1970s, with a large jump in the early 1980s due to an El Niño–induced precipitation decrease and subsequent increases primarily due to surface warming, while the very wet areas (PDSI $> +3.0$) have declined slightly. Together, the global areas in either very dry or very wet conditions decreased slightly by ~7% from 1950 to 1972, caused primarily by precipitation changes. Since 1972, the very dry or wet areas have increased from ~20% to 38% of the total land areas, with surface warming as the primary cause after the middle 1980s. During the last two–three decades, there was a tendency of more extreme (either very dry or very wet) conditions over many regions, including the United States, Europe, east Asia, southern Africa, and the Sahel. Surface air temperature increases over land, which increase the water-holding capacity of the air and thus its demand of moisture, have been a primary cause for the widespread drying during the last two–three decades.

Evapotranspiration in the Palmer model is calculated using a simple scheme that does not explicitly account for the effects of changes in surface solar radiation, relative humidity, and wind speed (Penman 1948). Surface solar radiation appears to have decreased over the United States and parts of Europe and Russia during 1961–90 (Abakumova et al. 1996; Liepert 2002). These decreases are often cited as the main cause (e.g., Roderick and Farquhar 2002) for the decreasing trends in "pan evaporation"—evaporation from water surface in a pan—since the late 1950s or early 1960s over the United States, parts of Europe, Siberia (Peterson et al. 1995), India (Chattopadhyay and Hulme 1997), and China (Liu et al. 2004).

Pan evaporation (E_{pa}) and actual evapotranspiration (E), however, exhibit complementary rather than proportional behavior such that, for regions with less than adequate moisture, E increases with potential evapotranspiration (consistent with the Palmer model) but decreases with E_{pa} (Brutsaert and Parlange 1998). For example, over the Mississippi River basin during the last 50 yr, increased cloudiness has decreased solar heating and thus pan evaporation, while actual evapotranspiration has increased because of increased precipitation and soil moisture (Milly and Dunne 2001). A recent reassessment of the evaporation data from the United States and the former Soviet Union (Golubev et al. 2001) suggests increasing trends in actual evaporation over southern Russia and most of the United States during the last 40 yr.

Our PDSI results, which are based on atmospheric moisture supply and demand near the surface, are consistent with increased evaporation under greenhouse gas–induced warming, as predicted by comprehensive coupled climate models (Cubasch et al. 2001; Dai et al. 2001). Global temperature increases have become pronounced after the 1970s (Folland et al. 2001) and have been attributed to human-induced climate changes arising primarily from increased greenhosue gases (Mitchell et al. 2001; Dai et al. 2001; Karl and Trenberth 2003). Higher temperatures increase the water-holding capacity of the atmosphere and thus increase potential evapotranspiration. Hence global warming not only raises temperatures, but also enhances drying near the surface, as is captured by the PDSI. The increased risk of drought duration, severity, and extent is a direct consequence (Trenberth et al. 2003), and the theoretical expectations are being realized, as shown here and discussed by Nicholls (2004).

Acknowledgments. This study was partly supported by NSF Grant ATM-0233568 and NCAR's Water Cycle Across Scales Initiative. [The PDSI dataset (updated to 2003) can be downloaded from http://www.cgd.ucar.edu/cas/catalog/climind/pdsi.html.]

REFERENCES

Abakumova, G. M., E. M. Feigelson, V. Russak, and V. V. Stadnik, 1996: Evaluation of long-term changes in radiation, cloudiness, and surface temperature on the territory of the former Soviet Union. *J. Climate,* **9,** 1319–1327.

Alley, W. M., 1984: Palmer Drought Severity Index: Limitations and assumptions. *J. Climate Appl. Meteor.,* **23,** 1100–1109.

Brutsaert, W., and M. B. Parlange, 1998: Hydrologic cycle explains the evaporation paradox. *Nature,* **396,** 30.

Chattopadhyay, N., and M. Hulme, 1997: Evaporation and potential evapotranspiration in India under conditions of recent and future climate change. *Agric. For. Meteor.,* **87,** 55–73.

Chen, M., P. Xie, J. E. Janowiak, and P. A. Arkin, 2002: Global land precipitation: A 50-yr monthly analysis based on gauge observations. *J. Hydrometeor.,* **3,** 249–266.

Cole, J. E., and E. R. Cook, 1998: The changing relationship between ENSO variability and moisture balance in the continental United States. *Geophys. Res. Lett.,* **25,** 4529–4532.

Cook, E. R., D. M. Meko, D. W. Stahle, and M. K. Cleaveland, 1999: Drought reconstructions for the continental United States. *J. Climate,* **12,** 1145–1162.

Cubasch, U., and Coauthors, 2001: Projections of future climate change. *Climate Change 2001: The Scientific Basis: The IPCC WG1 Third Assessment Report,* J. T. Houghton et al., Eds., Cambridge University Press, 525–582.

Dai, A. G., and T. M. L. Wigley, 2000: Global patterns of ENSO-induced precipitation. *Geophys. Res. Lett.,* **27,** 1283–1286.

——, and K. E. Trenberth, 2002: Estimates of freshwater discharge from continents: Latitudinal and seasonal variations. *J. Hydrometeor.,* **3,** 660–687.

——, I. Y. Fung, and A. D. Del Genio, 1997: Surface observed global

land precipitation variations during 1900–88. *J. Climate,* **10,** 2943–2962.
——, K. E. Trenberth, and T. R. Karl, 1998: Global variations in droughts and wet spells: 1900–1995. *Geophys. Res. Lett.,* **25,** 3367–3370.
——, T. M. L. Wigley, B. A. Boville, J. T. Kiehl, and L. E. Buja, 2001: Climates of the twentieth and twenty-first centuries simulated by the NCAR Climate System Model. *J. Climate,* **14,** 485–519.
——, P. J. Lamb, K. E. Trenberth, M. Hulme, P. D. Jones, and P. Xie, 2004: The recent Sahel drought is real. *J. Climatol.,* in press.
Dai, Y. J., and Coauthors, 2003: The Common Land Model. *Bull. Amer. Meteor. Soc.,* **84,** 1013–1023.
Domonkos, P., S. Szalai, and J. Zoboki, 2001: Analysis of drought severity using PDSI and SPI indices. *Idoejaras,* **105,** 93–107.
dos Santos, R. M. N., and A. R. Pereira, 1999: PALMER drought severity index for western Sao Paulo state, Brazil. *Rev. Bras. Agrometeor.,* **7,** 139–145.
Folland, C. K., and Coauthors, 2001: Observed climate variability and change. *Climate Change 2001: The Scientific Basis,* J. T. Houghton et al., Eds., Cambridge University Press, 99–181.
Fye, F. K., D. W. Stahle, and E. R. Cook, 2003: Paleoclimatic analogs to twentieth-century moisture regimes across the United States. *Bull. Amer. Meteor. Soc.,* **84,** 901–909.
Golubev, V. S., and Coauthors, 2001: Evaporation changes over the contiguous United States and the former USSR: A reassessment. *Geophys. Res. Lett.,* **28,** 2665–2668.
Groisman, P. Ya., R. W. Knight, T. R. Karl, D. R. Easterling, B. Sun, and J. H. Lawrimore, 2004: Contemporary changes of the hydrological cycle over the contiguous United States: Trends derived from in situ observations. *J. Hydrometeor.,* **5,** 64–85.
Guttman, N. B., J. R. Wallis, and J. R. M. Hosking, 1992: Spatial comparability of the Palmer drought severity index. *Water Resour. Bull.,* **28,** 1111–1119.
Heim, R. R., Jr., 2000: Drought indices: A review. *Drought: A Global Assessment,* D. A. Wilhite, Ed., Routledge, 159–167.
——, 2002: A review of twentieth-century drought indices used in the United States. *Bull. Amer. Meteor. Soc.,* **83,** 1149–1165.
Hollinger, S. E., and S. A. Isard, 1994: A soil moisture climatology of Illinois. *J. Climate,* **7,** 822–833.
Jones, P. D., and A. Moberg, 2003: Hemispheric and large-scale surface air temperature variations: An extensive revision and an update to 2001. *J. Climate,* **16,** 206–223.
Karl, T. R., 1986: Sensitivity of the Palmer Drought Severity Index and Palmer's Z-index to their calibration coefficients including potential evapotranspiration. *J. Climate Appl. Meteor.,* **25,** 77–86.
——, and A. J. Koscielny, 1982: Drought in the United States: 1895–1981. *J. Climatol.,* **2,** 313–329.
——, and R. W. Knight, 1998: Secular trends of precipitation amount, frequency, and intensity in the United States. *Bull. Amer. Meteor. Soc.,* **79,** 231–241.
——, and K. E. Trenberth, 2003: Modern global climate change. *Science,* **302,** 1719–1723.
Keyantash, J., and J. A. Dracup, 2002: The quantification of drought: An evaluation of drought indices. *Bull. Amer. Meteor. Soc.,* **83,** 1167–1180.
Kiladis, G. N., and H. F. Diaz, 1989: Global climatic anomalies associated with extremes in the Southern Oscillation. *J. Climate,* **2,** 1069–1090.
Liepert, B. G., 2002: Observed reductions of surface solar radiation at sites in the United States and worldwide from 1961 to 1990. *Geophys. Res. Lett.,* **29,** 1421, doi:10.1029/2002GL014910.
Liu, B., M. Henderson, M. Xu, and W. Gong, 2004: A spatial analysis of pan evaporation trends in China, 1955–2000. *J. Geophys. Res.,* in press.
Lloyd-Hughes, B., and M. A. Saunders, 2002: A drought climatology for Europe. *Int. J. Climatol.,* **22,** 1571–1592.
Milly, P. C. D., and K. A. Dunne, 2001: Trends in evaporation and surface cooling in the Mississippi River basin. *Geophys. Res. Lett.,* **28,** 1219–1222.
Mitchell, J. F. B., and Coauthors, 2001: Detection of climate change and attribution of causes. *Climate Change 2001: The Scientific Basis,* J. T. Houghton et al., Eds., Cambridge University Press, 695–738.
Monahan, A. H., and A. Dai, 2004: The spatial and temporal structure of ENSO nonlinearity. *J. Climate,* **17,** 3026–3036.
Nicholls, N., 2004: The changing nature of Australian droughts. *Climatic Change,* **63,** 323–336.
Ntale, H. K., and T. Y. Gan, 2003: Drought indices and their application to East Africa. *Int. J. Climatol.,* **23,** 1335–1357.
Palmer, W. C., 1965: Meteorological drought. Research Paper 45, U.S. Dept. of Commerce, 58 pp.
Penman, H. L., 1948: Natural evaporation from open water, bare soil and grass. *Proc. Roy. Soc. London,* **A193,** 120–145.
Peterson, T. C., V. S. Golubev, and P. Ya. Groisman, 1995: Evaporation losing its strength. *Nature,* **377,** 687–688.
Philip, J. R., 1957: Evaporation, and moisture and heat fields in the soil. *J. Meteor.,* **14,** 354–366.
Robock, A., and Coauthors, 2000: The Global Soil Moisture Data Bank. *Bull. Amer. Meteor. Soc.,* **81,** 1281–1299.
Roderick, M. L., and G. D. Farquhar, 2002: The cause of decreased pan evaporation over the past 50 years. *Science,* **298,** 1410–1411.
Ropelewski, C. F., and M. S. Halpert, 1987: Global and regional scale precipitation patterns associated with the El Niño/Southern Oscillation. *Mon. Wea. Rev.,* **115,** 1606–1626.
Thornthwaite, C. W., 1948: An approach toward a rational classification of climate. *Geogr. Rev.,* **38,** 55–94.
Trenberth, K. E., and T. J. Hoar, 1996: The 1990–1995 El Nino Southern Oscillation event: Longest on record. *Geophys. Res. Lett.,* **23,** 57–60.
——, and J. M. Caron, 2000: The Southern Oscillation revisited: Sea level pressures, surface temperatures, and precipitation. *J. Climate,* **13,** 4358–4365.
——, A. Dai, R. M. Rasmussen, and D. B. Parsons, 2003: The changing character of precipitation. *Bull. Amer. Meteor. Soc.,* **84,** 1205–1217.
——, J. T. Overpeck, and S. Solomon, 2004: Exploring drought and its implications for the future. *Eos, Trans. Amer. Geophys. Union,* **85,** 27.
Vinnikov, K. Y., and I. B. Yeserkepova, 1991: Soil moisture: Empirical data and model results. *J. Climate,* **4,** 66–79.
Webb, R. S., C. E. Rosenzweig, and E. R. Levine, 1993: Specifying land surface characteristics in general circulation models: Soil profile data set and derived water-holding capacities. *Global Biogeochem. Cycles,* **7,** 97–108.
Wilhite, D. A., 2000: Drought as a natural hazard: Concepts and definitions. *Droughts: A Global Assessment,* D. A. Wilhite, Ed., Routledge, 3–18.
Yang, D., B. Ye, and D. Kane, 2004: Streamflow hydrology changes over Siberian Yenisei River basin. *J. Hydrol.,* **296,** 59–80.